BMC Medical Imaging

RESEARCH

Open Access

A nomogram for diagnosis of BI-RADS 4 breast nodules based on three-dimensional volume ultrasound

Xianping Jiang[1†], Chen Chen[2,3,4†], Jincao Yao[2,3,4], Liping Wang[2,3,4], Chen Yang[2,3,4], Wei Li[2,3,4], Di Ou[2,3,4], Zhiyan Jin[5], Yuanzhen Liu[2,3,4], Chanjuan Peng[2,3,4], Yifan Wang[2,3,4*] and Dong Xu[2,3,4*]

Abstract

Objectives The classification of malignant breast nodules into four categories according to the Breast Imaging Reporting and Data System (BI-RADS) presents significant variability, posing challenges in clinical diagnosis. This study investigates whether a nomogram prediction model incorporating automated breast ultrasound system (ABUS) can improve the accuracy of differentiating benign and malignant BI-RADS 4 breast nodules.

Methods Data were collected for a total of 257 nodules with breast nodules corresponding to BI-RADS 4 who underwent ABUS examination and for whom pathology results were obtained from January 2019 to August 2022. The participants were divided into a benign group (188 cases) and a malignant group (69 cases) using a retrospective study method. Ultrasound imaging features were recorded. Logistic regression analysis was used to screen the clinical and ultrasound characteristics. Using the results of these analyses, a nomogram prediction model was established accordingly.

Results Age, distance between nodule and nipple, calcification and C-plane convergence sign were independent risk factors that enabled differentiation between benign and malignant breast nodules (all $P < 0.05$). A nomogram model was established based on these variables. The area under curve (AUC) values for the nomogram model, age, distance between nodule and nipple, calcification, and C-plane convergence sign were 0.86, 0.735, 0.645, 0.697, and 0.685, respectively. Thus, the AUC value for the model was significantly higher than a single variable.

Conclusions A nomogram based on the clinical and ultrasound imaging features of ABUS can be used to improve the accuracy of the diagnosis of benign and malignant BI-RADS 4 nodules. It can function as a relatively accurate predictive tool for sonographers and clinicians and is therefore clinically useful.

†Xianping Jiang and Chen Chen contributed equally to this work.

*Correspondence:
Yifan Wang
wangyf@zjcc.org.cn
Dong Xu
xudong@zjcc.org.cn

Full list of author information is available at the end of the article

Advances in knowledge statement we retrospectively analyzed the clinical and ultrasound characteristics of ABUS BI-RADS 4 nodules and established a nomogram model to improve the efficiency of the majority of ABUS readers in the diagnosis of BI-RADS 4 nodules.

Keywords Automated breast ultrasound system, Nomograms, Diagnosis, Breast nodules, BI-RADS classification, Predictive models

Introduction

Breast cancer is currently the number-one cause of cancer-related death in women, ranking first in terms of both new cases and deaths [1–3], and as such it represents a serious threat to the physical and mental health of women worldwide. Many factors have been found to influence the occurrence and development of breast cancer, including genetic, endocrine, lifestyle and social factors, cultural background, and aspects of the built environment in which a participant lives [4]. A variety of therapies, including surgery, radiation therapy, chemotherapy, endoscopic therapy and immunotherapy, are available for the treatment of breast cancer [5, 6]; however, its mortality rate remains significant [2, 7, 8]. Early screening, early diagnosis and appropriate therapy are therefore key to improving the prognosis, quality of life and survival rate of breast cancer participants.

The fifth edition of the Breast Imaging-Reporting and Data System (BI-RADS) has been widely used in clinical work, increasing the consistency of the clinical approach across regions and among different levels of hospital and different doctors, so that sonographers can produce more accurate and standardized ultrasound reports. It is also convenient for sonographers and clinicians in various departments to adopt a common standard, objectively analyzing and exchanging participant information, and this helps to guide subsequent clinical decision-making and treatment. However, the proportion of breast BI-RADS 4 nodules that are found to be malignant varies from 2–95% [9], highlighting the difficulty of ultrasound diagnosis. Therefore, accurately distinguishing between benign and malignant characteristics among the breast BI-RADS 4 nodules in ultrasound diagnosis is both crucial and challenging.

Automated breast ultrasound system (ABUS) is a three-dimensional ultrasound breast-imaging technique. Its unique volume imagery and multi-planar reconstruction enable the location of nodules in the breast to be determined to a higher degree of accuracy, and the relationship with surrounding tissues to be more clearly visible, providing more diagnostic information for breast diseases. At the same time, the scanning procedure, which can be separated from the rest of the process, can be performed by a technician. In addition, the full volume of the breast is recorded, making repeated and comparative readings possible [10]. Studies in clinical practice have shown that in female participants with dense breast tissue, the use of ABUS leads to increased specificity in the diagnosis of breast cancer [11]. Its detection rate for breast lesions is comparable to that of handheld ultrasound [12]. The use of ABUS can also facilitate preoperative planning and save physicians significant time relative to the use of handheld ultrasound in symptomatic out-participants and the feasibility evaluation of response control for neoadjuvant treatment of breast cancer [13, 14]. The application of ABUS is an effective screening modality for breast cancer [15]; however, the combination of full-field digital mammography with three-dimensional ABUS significantly improves and increases breast cancer detection rates in women with high breast density, including small and invasive cancers [16, 17]. A disadvantage of ABUS is that obtaining a large number of images sharply increases the reading volume for ultrasound diagnostic physicians. To alleviate this burden, researchers are working to combine ABUS with artificial intelligence for a number of applications, including the automatic identification of tumor lesions, tumor segmentation, tumor volume calculation, fully automated BI-RADS classification, and benign and malignant classification [18–27]. It has also been shown that the use of new deep learning networks combined with automatic segmentation networks for morphological analysis can help physicians to improve their accuracy in the diagnosis of breast cancer [28]. However, offline analysis and familiarity with AI operations and processes are required, and the use of this procedure is therefore unfeasible for the majority of sonographers, especially those in remote areas. There is an urgent need for a natural, objective, straightforward, and intuitive method that does not depend on costly equipment or sophisticated operational technology to assist ABUS imaging diagnosticians in enhancing work efficiency and diagnostic accuracy. This would facilitate the development of more reasonable treatment plans during subsequent clinical evaluations. As a significant data visualization instrument, the nomogram possesses distinct advantages in data analysis and interpretation. It effectively visualizes the relationships among variables, customizes calculations, quantifies variable contributions, and ultimately provides decision support.

In this study, we performed a retrospective analysis of the clinical and ultrasound characteristics associated with ABUS BI-RADS 4 nodules. Based on this analysis, we developed a nomogram model designed to enhance diagnostic efficiency and consistency among ABUS

readers in differentiating between benign and malignant BI-RADS 4 nodules. The primary goal is to improve diagnostic accuracy.

Participants and methods

General information

Data for a total of 233 female participants with breast masses were retrospectively collected from the Department of Breast Oncology at the Hospital, for the period January 2019 to August 2022. It was approved by the Ethics Committee of the Hospital. Informed consent from the participants was exempted (IRB- 2022 – 202).The nodules were classified as BI-RADS 4 by ABUS, and diagnoses were confirmed by surgery or core needle biopsy. The age ranged from 20 to 86 years, with an average of 46.72 ± 11.36 years (see Table 1 for details). All participants voluntarily underwent breast ABUS.

Inclusion and exclusion criteria

Inclusion criteria: (1) Breast nodules categorized as BI-RADS 4 A, 4B, or 4 C based on the fifth edition of the ultrasound BI-RADS classification system, as assessed using ABUS images by two senior attending physicians. If the readings of the two radiologists were discordant, a final consensus was reached through a collaborative review of the case. (2) No prior radiotherapy, chemotherapy, or other treatments administered before the ABUS examination; (3) Pathological results of breast nodules obtained through core needle biopsy or excisional biopsy; (4) The interval between the ABUS examination and pathological confirmation was within one week.

Exclusion criteria: (1)Unclear pathological findings; (2) Multiple lesions in a single breast that are closely located or exhibit differing benign and malignant characteristics; (3) Target lesions not fully visible on ABUS imaging; (4) Participant refusal to undergo ABUS examination or inability to complete a comprehensive scan due to local skin rupture or other limitations.

Instruments and image acquisition methods

Instrument used GE Invenia ABUS (General Electric Company, Country of Production: Wuxi, Jiangsu, China). Image acquisition is conducted by technical specialists with over five years of professional experience. The procedure for image acquisition is outlined as follows: The participant's data, including their ultrasound number, name, and date of birth are input into the ABUS system. The participant is asked to lie in a supine position and fully expose the breast, axilla and subclavian area. The arm closest to the breast under examination is raised and bent above the head, the head is tilted to the opposite side, a latex triangle pad is placed on the participant's back, and a towel is placed behind the scapula. The axilla is flattened so that the breast tissue is evenly distributed across the chest wall of the side under examination, the slope is as even as possible in all directions, and the tissue is not unevenly accumulated or tilted. The nipple is orientated toward the ceiling. Before scanning from multiple views (see below), a coupling agent is evenly applied to the whole breast using a silicone scoop––the amount applied to the areola and nipple area must be sufficient to avoid leaving gaps, preventing any attenuation of the echo. The appropriate scanning area is selected according to the participant's breast size, the window width and window level are adjusted, the image is optimized, and the pressure is adjusted to the maximum level that is acceptable to the participant. The participant is asked to maintain the position, breathe slowly, and try to achieve a good fit between the probe and the surface of the breast. Three standard views of both breasts––the anteroposterior position (AP), the lateral position (LAT), and the medial position (MED)––are used, scanning from the foot side to the head side, with a scan time of about 40 s and a slice thickness of 0.5 mm for each view. If the breast is too large and the lesion is close to the edge of the gland, one or more of the following additional views can be added to the scanning view sequence to ensure that the examination covers all breast tissue: upper (SUP), lower (INF), outer upper quadrant (UOQ), outer lower quadrant (LOQ), inner upper quadrant (UIQ), axillary (Axilla). At the end of the scan, image quality is evaluated to confirm the completion of the scan, and the image data are saved and sent to the image analysis workstation.

Table 1 General characteristics of the nodules (i.e. benign and malignant)

Classification of BI-RADS	Pathological nature	Number of cases	Age (year, $\bar{x}\pm s$)	Maximum diameter of nodule [cm, M(Q1, Q3)]	Volume of nodule [ml, M(Q1, Q3)]	Distance from nipple [cm, M(Q1, Q3)]	Distance from epidermis [cm, M(Q1, Q3)]
4A	Benign	179	44.20 ± 10.40	0.94(0.73,1.40)	254.80(105.01,614.04)	3.30(2.02,4.70)	1.13(0.90,1.39)
4A	Malignant	22	49.05 ± 11.50	1.49(1.18,2.16)	1019.90(537.70,2596.02)	4.38(2.49,6.34)	1.23(0.97,1.48)
4B	Benign	9	40.56 ± 13.59	1.32(1.07,2.57)	937.90(384.11,2380.00)	3.84(2.35,6.73)	1.00(0.90,1.29)
4B	Malignant	19	53.05 ± 8.73	1.51(1.23,2.30)	1072.21(554.15,3683.68)	4.15(2.78,5.58)	1.17(0.90,1.55)
4C	Benign	0					
4C	Malignant	28	56.21 ± 9.34	2.07(1.70,3.43)	2768.92(1544.20,5674.50)	4.75(3.43,6.22)	1.40(1.27,1.73)

After acquiring the images, the participant's age was recorded, along with the following characteristics for each nodule: location, maximum diameter, distance from nipple and epidermis, shape, orientation, boundary, edge, internal echo, posterior echo, calcification, C-plane convergence sign, relationship with catheter, and jump sign. Ultrasound characteristics such as irregular shape, vertical orientation, indistinct or blurred margins, uneven or spiculated edges, differential lobulation, calcification, acoustic shadowing, and C-plane convergence are considered suspicious signs of malignancy. According to the fifth edition of the BI-RADS classification system, breast lesions are categorized into one of seven categories based on their ultrasound features. Category 0 is assigned for cases requiring additional imaging due to incomplete assessment. Category 1 indicates a negative result; Category 2 signifies benign findings; Category 3 denotes probably benign lesions with a likelihood of malignancy not exceeding 2%. Category 4 is classified as suspicious and encompasses a malignancy probability ranging from greater than 2% to less than 95%, further subdivided into three subcategories: 4 A (2–10% likelihood of malignancy, one suspicious sign), 4B (10–50% likelihood of malignancy, two suspicious signs), and 4 C (50–95% likelihood of malignancy, three suspicious signs). Category 5 is highly suggestive of malignancy with a probability of at least 95%, recommending tissue diagnosis. Category 6 represents biopsy-proven malignancy. Pathology test results, including lymph node metastasis, were reviewed and documented.

Statistical methods

IBM SPSS Statistics version 22.0 (IBM Corp., Armonk, NY) was used to analyze the data. The Shapiro–Wilk test was used to inspect the measurement data, which was found to exhibit a normal distribution with variance expressed as ±*s*. Comparisons between groups used the independent samples *t*-test. The maximum diameter, volume, distance to the nipple, and distance to the epidermis ($P<0.05$) of nodules with skewed distribution and uneven variance were expressed in terms of their *M (IQR)*, and comparisons between the groups were performed using the non-parametric Wilcoxon Mann–Whitney rank sum test. Count data were expressed as case (%). Pearson chi-square, continuous correction chi-square, or Fisher's exact test were used to compare the differences between the participant groups (benign and malignant signs in ABUS findings). For the univariate binary logistic analysis of the characteristics listed above, $P<0.05$ was used as the threshold for statistical significance; the same threshold was used for the multivariate binary logistic regression analysis and in establishing a nomogram prediction model.

Results

Participant characteristics

The mean age for the benign group was 44.03 ± 10.56 years, and the mean age for the malignant group was 53.06 ± 10.24 years. There was a significant difference in mean age between the two groups ($t=6.120$, $P<0.01$), and the 95%CI for the mean difference was 6.12–11.93.

Clinicopathological types of BI-RADS 4 nodules

The clinicopathological results for the 257 nodules were as follows: there were 188 benign nodules (benign group), including 77 cases of breast adenosis (40.96%), 48 cases (25.53%) of fibroadenoma, 40 cases (21.28%) of breast adenosis with fibroadenoma, 18 cases (9.57%) of intraductal papilloma, 3 cases (1.60%) of inflammatory nodules, and 2 cases of cyst with infection (1.06%). There were 69 malignant nodules (malignant group), including 60 cases of invasive cancer (86.96%), 3 cases of ductal carcinoma in situ (4.34%), 2 cases of microinvasive carcinoma (2.90%), 2 cases of mucinous carcinoma (2.90%), 1 case of lymphoma (1.45%), and 1 case (1.45%) of solid papillary carcinoma.

ABUS ultrasound features of benign and malignant BI-RADS 4 nodules

There were statistically significant differences ($P<0.05$) in the maximum diameter, nodule volume, and distance from the nipple and epidermis between the two groups, as shown in Table 2. There were also significant differences ($P<0.05$) between the two groups in terms of the following ultrasound characteristics of the nodules: shape, orientation, boundary, margin, internal echo, calcification, C-plane convergence sign and pathological lymph node metastasis. There were no significant

Table 2 General characteristics of the two groups of nodules (i.e. benign and malignant)

Group	Number of cases	Age (year, $\bar{x}\pm s$)	Maximum diameter of nodule [cm, M(Q1, Q3)]	Volume of nodule [ml, M(Q1, Q3)]	Distance from nipple [cm, M(Q1, Q3)]	Distance from epidermis [cm, M(Q1, Q3)]
Benign	188	44.03 ± 10.56	1.00(0.74,1.45)	265.23(109.35,659.88)	3.32(2.02,4.80)	1.13(0.90,1.38)
Malignant	69	53.06 ± 10.24	1.70(1.30,2.50)	1822.86(864.74,3683.68)	4.59(2.92,6.01)	1.33(1.04,1.60)
Total	257	46.72 ± 11.36	1.19(0.81,1.72)	411.84(149.09,1399.02)	3.62(2.21,5.22)	1.19(0.95,1.40)
t/Z value		*t* = -6.120	Z = 7.032	Z = 8.23	Z = 3.172	Z = -3.224
P value		<0.01	<0.01	<0.01	0.02	0.001

differences ($P > 0.05$) between the two groups in terms of nodule location, posterior echo, peripheral duct dilatation, connection with the duct, location in the duct, or jump sign (see Tables 2 and 3 for details). Univariate logistic regression analysis showed that age, maximum diameter, volume, distance from nipple and epidermis, shape, orientation, margin, boundary, internal echo, calcification, and C-plane convergence sign were statistically significant ($P < 0.05$) in the diagnosis of benign and malignant nodules (see Table 4 for details).

Construction of the nomogram model

Multivariate logistic regression analysis showed that participant age had a statistically significant effect on the diagnosis of benign and malignant breast nodules ($OR = 1.088$, 95% CI: 1.052–1.154, $P < 0.01$). The distance between the nodule and the nipple was statistically significant in the diagnosis of benign and malignant breast nodules ($OR = 1.023$, 95% CI: 1.002–1.045, $P = 0.033$). The presence/absence of calcification was found to be statistically significant in the diagnosis of benign and malignant breast nodules ($OR = 6.722$, 95% CI: 2.606–17.336, $P < 0.01$). C-plane convergence sign was found to be statistically significant in the diagnosis of benign and malignant breast nodules ($OR = 10.819$, 95% CI: 2.483–47.137, $P = 0.002$). Based on these key independent factors, a nomogram model for predicting whether BI-RADS 4 breast nodules were benign or malignant based on ABUS findings was established (Fig. 1).

Validation of the nomogram model

Internal validation was conducted using leave-one-out cross validation with 2000 3-fold, 5-fold, and 10-fold iterations. The average C-index values were found to be 0.849, 0.851, and 0.851, respectively. The AUC values for the nomogram model, age, distance between nodule and nipple, calcification, and C-plane convergence sign were 0.86, 0.735, 0.645, 0.697, and 0.685, respectively (Fig. 2). Thus, the AUC value for the model was significantly higher than that of any single variable (i.e. 0.735, for age) in predicting benign and malignant nodules.

Examples of applications of the nomogram model

A nomogram was used to predict whether BI-RADS 4 nodules were benign or malignant based on ABUS findings, by adding straight vertical lines to the plot (Fig. 3). Lines were drawn for the point-to-point axis scores for each factor (age, red line; distance from nipple, blue line; calcification, yellow line; C-plane convergence sign, green line). The total score for each predictor was then calculated. Finally, a total score line (purple) was added to obtain a prediction of the risk of malignancy. For example, for the case illustrated in Fig. 3A–C, a 59-year-old participant with a left breast mass gives a score of 56; the distance from the nipple was 59.6 mm, corresponding to a score of 22; calcification was present, corresponding to score of 32.5; and the C-plane convergence sign corresponded to a score of 51. The total score was therefore 162.5 ($56 + 22 + 32.5 + 52$). The nomogram predicted a probability of malignancy > 90%, and pathology tests confirmed invasive breast cancer. In the case illustrated in Fig. 3D–F, a 29-year-old participant with a right breast mass gives a score of 13; the distance from the nipple was 51.9 mm, corresponding to a score of 19; and calcification was present, corresponding to a score of 32. There was no C-plane convergence (score of 0). The total score was thus 64 ($13 + 19 + 32 + 0$). The nomogram predicted that the probability of malignancy was < 20%, and pathology tests confirmed breast fibroadenoma.

Discussion

Ultrasound is the first-line imaging technique for breast cancer screening. X-ray examinations involve radiation, discomfort and a relatively low nodule detection rate in dense breast tissue, while handheld ultrasound produces no radiation and does not cause discomfort, and the type of breast tissue does not affect the detection rate. Magnetic resonance imaging is expensive, and handheld ultrasound is preferable for breast disease screening for a multitude of reasons, including its low cost, convenience, and real-time dynamics. However, handheld ultrasound does have its disadvantages: there are marked differences in the quality of the scans available in different geographical regions and those produced by different operators, and the images of the whole scan cannot be saved. ABUS is capable of overcoming these shortcomings. The full volume and unique C-plane imaging is favored by the majority of doctors and is beneficial for most participants. The image for the full scanning volume can be preserved, repeatability is greatly improved, and pre- and post-lesion comparisons have become more objective, rendering the reported ultrasonographic characteristics of the same nodule and the diagnosis of benign and malignant nodules more consistent among doctors of different levels of seniority across different regions. In addition, the separation of scanning and diagnosis is possible, reducing dependence on the operator, greatly reducing the workload of the sonographer, and improving workflow [10]. Several studies have shown that the diagnostic accuracy of benign and malignant nodules achieved using ABUS is comparable to that of handheld ultrasound [29–31]. ABUS is a standardized method; however, one of its disadvantages is that it takes a considerable amount of time for sonographers to read the images, resulting in increased false negative rates [32]. The use of the four variables that were selected for inclusion in the nomogram prediction model can greatly reduce reading time and help to improve accuracy.

Table 3 Comparison of ABUS ultrasound features of the two groups of nodules (i.e. benign and malignant)

ABUS ultrasound features	Total	Benign	Malignant	χ^2/H/F	*P* value
Left/Right side (*n*, %)					
Left	121(47.1)	85(45.2)	36(52.2)	0.982	0.328
Right	136(52.9)	103(54.2)	33(47.8)		
Quadrant (*n*, %)					
UOQ	113(44.0)	80(42.6)	33(47.8)	0.083	0.773[a]
LOQ	52(20.2)	42(22.3)	10(14.5)		
UIQ	73(28.4)	52(27.7)	21(30.4)		
LIQ	19(7.4)	14(7.4)	5(7.2)		
Form (*n*, %)					
Oval/Round	84(32.7)	75(39.9)	9(13.0)	16.539	<0.01
Irregular shape	173(67.3)	113(60.1)	60(87.0)		
Orientation (*n*, %)					
Parallel	206(80.2)	167(85.6)	45(65.2)	13.233	<0.01
Vertical	51(19.8)	27(14.4)	24(34.8)		
Boundary (*n*, %)					
Clear	125(48.6)	108(57.4)	17(24.6)	21.749	<0.01
Unclear	132(51.4)	80(42.6)	52(75.4)		
Boundary (*n*, %)					
Smooth	98(38.1)	88(46.8)	10(14.5)	15.153	<0.01[a]
Unsmooth	27(10.5)	21(11.2)	6(8.7)		
Angulation	10(3.9)	3(1.6)	7(10.1)		
Micro segmented lobe	26(10.1)	15(8.0)	11(15.9)		
Burr	20(7.8)	9(4.8)	11(15.9)		
Vague	76(29.6)	52(27.7)	24(34.8)		
Internal echo (*n*, %)					
Hypoecho	217(84.4)	164(87.2)	53(76.8)	4.172	0.041
Mixed echo	40(15.6)	24(12.8)	16(23.2)		
Echo from the rear (*n*, %)					
Undamped	227(88.3)	164(87.2)	63(91.3)	0.824	0.364[a]
Damping	24(9.3)	19(10.1)	5(7.2)		
Enhance	6(2.3)	5(2.7)	1(1.4)		
Agent of calcification (*n*, %)					
None	171(66.5)	145(77.1)	26(37.7)	35.275	<0.01
Yes	86(33.5)	43(22.9)	43(62.3)		
Features of C convergence of planes (*n*, %)					
None	226(87.9)	184(97.2)	42(60.9)	65.154	<0.01
Yes	31(12.1)	4(2.1)	27(30.1)		
Peripheral duct dilatation (*n*, %)					
None	246(95.7)	177(94.1)	69(100)	2.911	0.088 [b]
Yes	11(4.3)	11(5.9)	0(0)		
Connected to a conduit (*n*, %)					
None	251(97.7)	183(97.3)	68(98.6%)	0.011	0.918 [b]
Yes	6(2.3)	5(2.7)	1(1.4%)		
Medial to the catheter (*n*, %)					
None	247(96.1)	178(94.7)	69(100)	2.529	0.112 [b]
Yes	10(3.9)	10(5.3)	0(0)		
Sign of jump (*n*, %)					
None	255(99.2)	186(99.5)	68(98.6)		0.466[c]
Yes	2(0.8)	1(0.5)	1(1.4)		
Lymphatic metastasis (*n*, %)					
None	245(95.3)	188(100)	57(82.6)	30.501	<0.01 [b]
Yes	12(4.7)	0(0)	12(17.4)		

Note: [a]Using Kruskal Waillis H-test; [b]Using continuous correction chisquare; [c]Using Fisher's exact probability method

Table 4 Results of univariate logistic regression analysis

variate	B	SE	Wald	*P* value	OR value	95%CI	
						Lower limit	Upper limit
Age	0.085	0.016	28.134	< 0.01	1.088	1.055	1.123
Maximum diameter of nodule	0.079	0.016	25.504	< 0.01	1.082	1.050	1.116
Volume of nodule	< 0.01	< 0.01	11.108	0.001	1.000	1.000	1.000
Distance from nipple	0.023	0.007	11.768	0.001	1.023	1.010	1.037
Distance from epidermis	0.070	0.033	4.413	0.036	1.072	1.005	1.145
Form	1.487	0.387	14.749	< 0.01	4.425	2.071	9.452
Orientation	1.157	0.327	12.494	< 0.01	3.180	1.674	6.041
Margin	0.263	0.069	14.690	< 0.01	1.300	1.137	1.487
Boundary	1.418	0.316	20.149	<0.01	4.129	2.223	7.670
Internal echo	0.724	0.359	4.060	0.044	2.063	1.020	4.172
Calcification	1.719	0.303	32.151	<0.01	5.577	3.079	10.102
Features of C convergence of planes	3.387	0.562	36.267	<0.01	29.571	9.821	89.039
Lymphatic metastasis	22.396	11602.711	< 0.01	0.998	5,328,232,815	< 0.01	

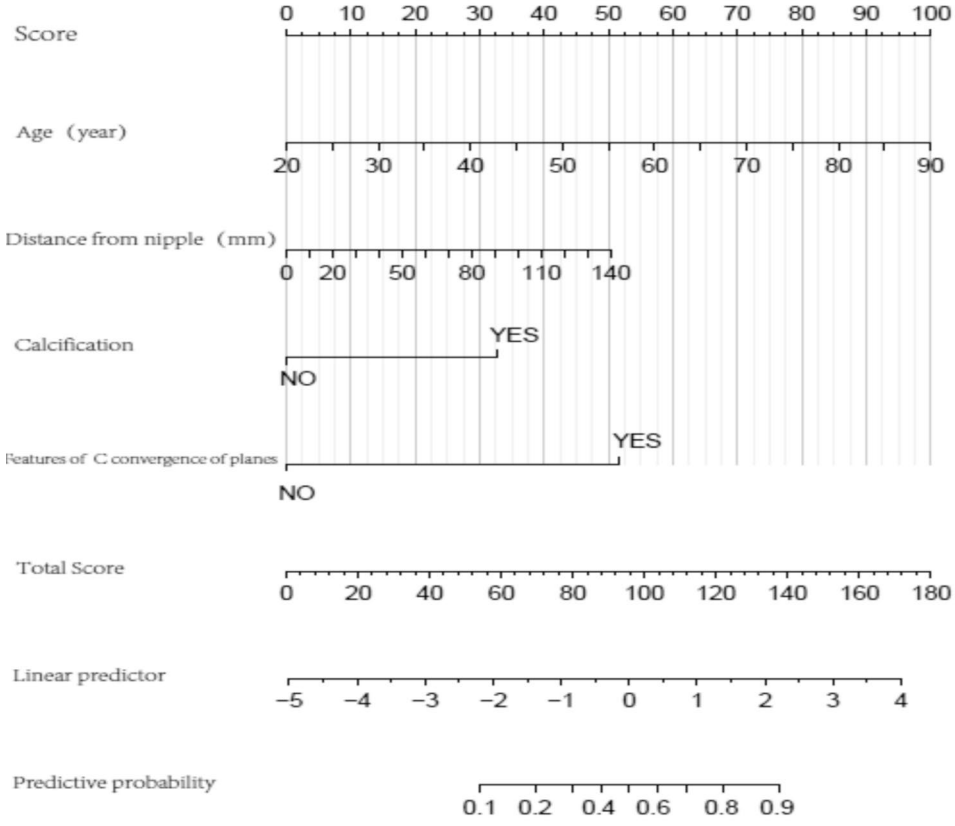

Fig. 1 Nomogram prediction model for benign and malignant BI-RADS 4 breast nodules based on ABUS findings

Improving the early detection rate is key to improving 5-year breast cancer survival rates, and accurate diagnosis of benign and malignant nodules in BI-RADS 4 cases is essential to improving the early detection rate [33]. The fifth edition of the BI-RADS classification has been widely used in clinical work involving breast nodules, but the description of lesion characteristics and the final I-RADS classification results largely depend on the experience and technical skill of the diagnostic physician [9]. Researchers are currently working to combine ABUS and artificial intelligence with the objective of realizing fully automated segmentation, detection and BI-RADS classification of masses on ABUS imaging [18, 25–27]. A study of dedicated computer-aided detection software for ABUS showed improved breast cancer detection rates for radiologists screening for breast cancer [34]. This approach has also been shown to reduce the frequency of misdiagnosis, especially for non-lumpy lesions of the breast [35]. However, it requires specific equipment and technical support, and it may therefore be difficult to

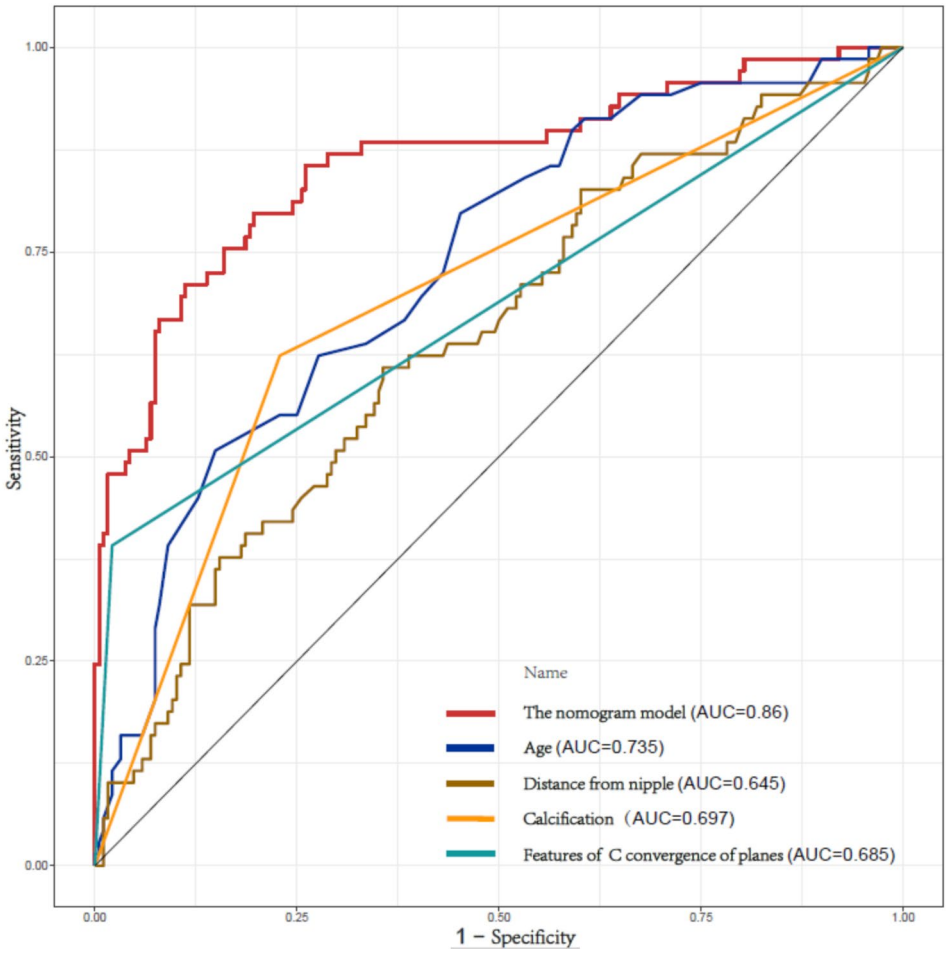

Fig. 2 Nomogram model and receiver operating curves for independent dependent variables

implement in rural hospitals and remote areas. Previous studies have demonstrated that clinical prediction models incorporating molecular subtyping, tumor size, and Cooper's ligament status effectively assess the tumor burden in axillary lymph nodes, supporting personalized breast cancer diagnosis and treatment decisions [36]. In this study, we integrated imaging and clinical characteristics of ABUS and incorporated variables that demonstrated statistical significance in distinguishing benign from malignant nodules through univariate logistic analysis into a multivariate logistic regression model. Notably, this is the first study to integrate participants' age, three-dimensional nodule location, and ABUS-specific imaging features. We developed a nomogram model for evaluating the malignancy risk of BI-RADS Category 4 nodules, transforming complex prediction results into graphical form to enhance the transparency of the diagnostic process and provide an innovative tool for breast cancer screening.

In this study, four independent risk factors were identified for differentiating between benign and malignant breast nodules: participant age, distance from the nodule to the nipple, presence of calcification, and the C-plane convergence sign. Based on these variables, a nomogram model was developed, demonstrating excellent diagnostic performance in internal validation, with an area under the Receiver Operating Characteristic(ROC)curve AUC of 0.86. This finding highlights the model's strong predictive capability in distinguishing between benign and malignant nodules, offering reliable decision support for clinical practice. Compared to traditional BI-RADS parameters, such as boundary and edge characteristics, which are often influenced by the experience and skills of diagnostic physicians, the variables included in this model-particularly participant age and nodule-to-nipple distance-are entirely objective. The inclusion of these objective indicators minimizes diagnostic bias arising from individual variability, thereby improving the reliability and reproducibility of the model's results. Calcification, a key imaging feature in breast nodule diagnostics, was simplified in this study to a binary variable (presence or absence) rather than being classified into microcalcifications or coarse calcifications. While this simplification may not fully capture the subtle differences between

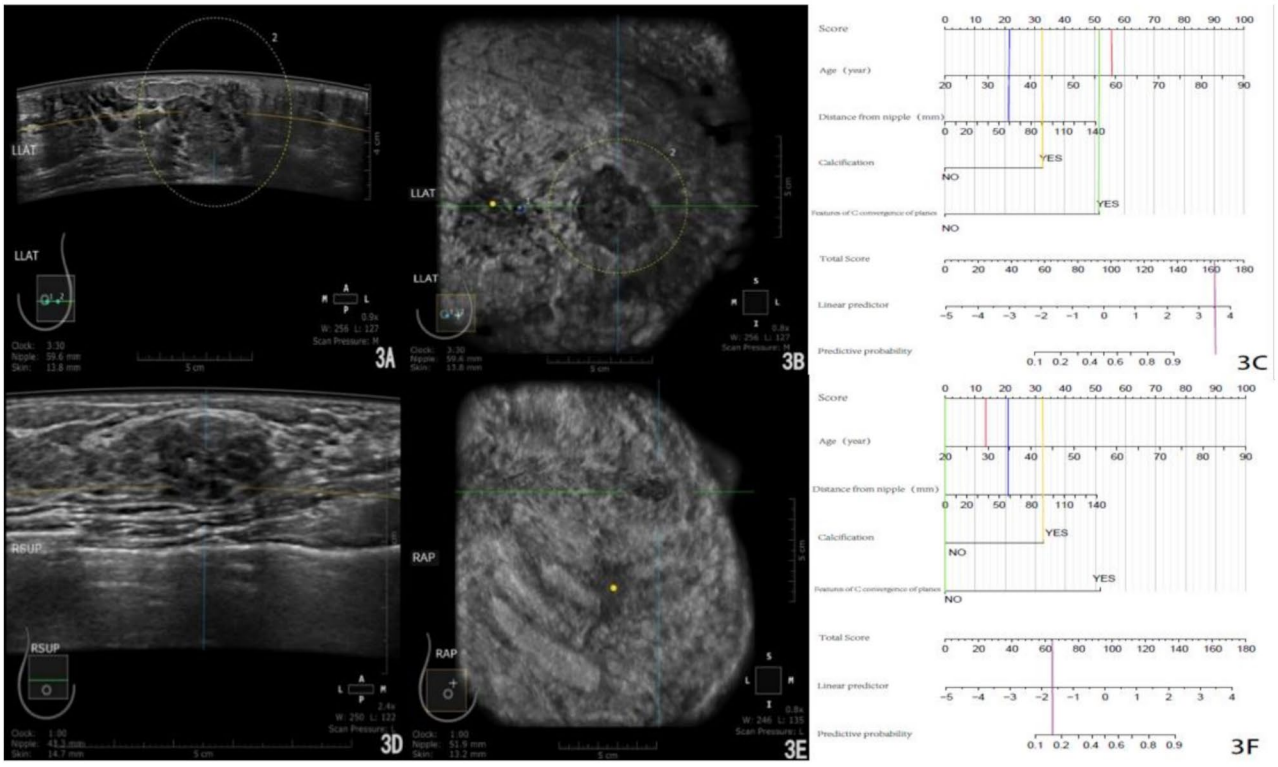

Fig. 3 Application of the nomogram model to predict whether BI-RADS 4 nodules were benign or malignant based on ABUSfindings. In the 59-year-old female participant with invasive breast cancer: (**3A**) The coronal view of ABUS reveals calcifications. (**3B**) The sagittal section of ABUS shows both calcifications and C-plane convergence sign. (**3C**) Using a nomogram model, the total score for the list of masses was calculated to be 162.5, indicating a malignancy risk value of > 0.9, which suggests a high likelihood of malignancy. In the 29-year-old female participant with breast fibroadenoma: (**3D**) The coronal view of ABUS also reveals calcifications. (**3E**) The sagittal section of ABUS shows calcifications without any C-plane convergence sign. (**3F**) According to the nomogram model, the total score for the mass was 64, with a malignancy risk value of < 0.2, suggesting a benign tumor.

calcification types, it significantly enhances the model's objectivity and reduces the subjectivity associated with calcification assessment by physicians. This approach is particularly advantageous in resource-limited settings, where streamlined and actionable diagnostic tools are critical. The C-plane convergence sign, a unique imaging feature of ABUS, further contributes to the model's diagnostic accuracy. Its straightforward and quantifiable nature not only underscores the advantages of ABUS technology but also improves the model's consistency and applicability. Importantly, the nomogram model is characterized by its intuitive design and broad applicability. Its independence from advanced technologies, expensive equipment, and highly specialized personnel makes it particularly suitable for use in primary healthcare settings and resource-constrained environments. By simplifying diagnostic workflows and standardizing predictive results, the model helps reduce the workload of diagnostic physicians while improving the efficiency and quality of breast nodule screening.

Limitations of this study are as follows. There is inevitable selection bias in this study. We included nodules with a confirmed pathological diagnosis, but most BI-RADS 1–3 nodules did not require pathological examination. Moreover, it has the most significance in predicting the benign and malignant BI-RADS 4 nodules. So, only BI-RADS 4 nodules were selected in this study. It is a single-center retrospective study with a relatively small number of cases, which may lead to bias in the results. Due to the insufficient number of cases, the nodules were divided into benign and malignant groups according to the results of pathology tests only, and no statistical analysis was performed for BI-RADS 4 nodules according to different pathological types. The same mass was not judged and measured by different senior doctors. Calcification was reported only as present or absent, without specific differentiation between coarse calcification and microcalcification. The nomogram used in this study was only internally validated, and although the validation showed a high level of consistency, we hope that multi-center data will be used for external validation in future studies.

Conclusion

In conclusion, age, distance between the nodule and the nipple, calcification, and C-plane convergence sign are independent risk factors that can be used to predict

malignancy in BI-RADS 4 nodules using ABUS. The nomogram model based on these factors is a useful tool. It can alleviate the workload of ultrasound physicians, substantially enhance the work efficiency of ABUS imaging diagnostic specialists, assist in improving the accuracy of diagnosing benign and malignant nodules, and provide robust evidence for clinical follow-up, thereby facilitating the development of rational treatment plans.

Abbreviations

BI-RADS	Breast Imaging Reporting and Data System
ABUS	Automated Breast Ultrasound System
AP	Anteroposterior position
LAT	Lateral position
MED	Medial position
UOQ	Outer upper quadrant
LOQ	Outer lower quadrant
UIQ	Inner upper quadrant
Axilla	Axillary
AUC	Area under the ROC curve
ROC	Receiver operating characteristic

Acknowledgements
Not applicable.

Author contributions
Xianping Jiang. Conceptualization, Methodology, Validation, Investigation, Writing - Original Draft. Chen Chen. Data curation, Project administration, Writing- Reviewing and Editing. Jincao Yao. Visualization, Investigation, Data Curation. Liping Wang. Supervision, Funding acquisition. Chen Yang. Software, Validation, Funding acquisition. Wei Li. Writing- Reviewing and Editing, Funding acquisition. Di Ou. Project administration. Zhiyan Jin. Software. Yuanzhen Liu. Supervision. Chanjuan Peng. Investigation. Yifan Wang. Data curation, Project administration. Dong Xu. Funding acquisition, Funding acquisition, Supervision, Conceptualization.

Funding
This work was supported by the "Pioneer" and "Leading Goose" R&D Program of Zhejiang Province (No. 2023C04039), the Zhejiang Provincial Medical and Health Science and Technology Program (No. 2022KY699, 2022KY661, 2023KY561 and 2025KY1676).

Data availability
The datasets generated and/or analysed during the current study are not publicly available due privacy but are available from the corresponding author on reasonable request.

Declarations

Ethics approval and consent to participate
This retrospective study's protocol was approved by the Independent Ethics Committee of Zhejiang Cancer Hospital (NO: IRB-2022-202), and written informed consent from the participant was waived by the ethics committee of the Independent Ethics Committee of Zhejiang Cancer Hospital (NO: IRB-2022-202). Participant records were anonymized and deidentified before analysis. We confirm that all methods were performed in accordance with the relevant guidelines and regulations.

Consent for publication
Not applicable.

Competing interests
The authors declare no competing interests.

Author details
[1]Department of Ultrasound, Shengzhou People's Hospital (Shengzhou Branch of the First Affiliated Hospital of Zhejiang University School of Medicine, the Shengzhou Hospital of Shaoxing University), Shengzhou 312400, China
[2]Department of Diagnostic Ultrasound Imaging & Interventional Therapy, Zhejiang Cancer Hospital, Hangzhou Institute of Medicine (HIM), Chinese Academy of Sciences, No.1 East Banshan Road, Gongshu District, Hangzhou, Zhejiang 310022, China
[3]Center of Intelligent Diagnosis and Therapy (Taizhou), Hangzhou Institute of Medicine (HIM), Chinese Academy of Sciences, Taizhou 317502, China
[4]Wenling Institute of Big Data and Artificial Intelligence in Medicine, Taizhou 317502, China
[5]Postgraduate training base Alliance of Wenzhou Medical University, Hangzhou 310022, China

Received: 19 July 2023 / Accepted: 3 February 2025
Published online: 14 February 2025

References

1. Loibl S, Poortmans P, Morrow M, Denkert C, Curigliano G. Breast cancer. Lancet. May 8.2021;397(10286):1750–1769. https://doi.org/10.1016/S0140-6736(20)32381-3
2. Siegel RL, Miller KD, Fuchs HE, Jemal A, Cancer statistics. 2022. CA: a cancer journal for clinicians. Jan 2022;72(1):7–33. https://doi.org/10.3322/caac.21708
3. Bray F, Ferlay J, Soerjomataram I, Siegel RL, Torre LA, Jemal A. Nov. Global cancer statistics 2018: GLOBOCAN estimates of incidence and mortality worldwide for 36 cancers in 185 countries. CA: a cancer journal for clinicians. 2018;68(6):394–424. https://doi.org/10.3322/caac.21492
4. McCormack V, McKenzie F, Foerster M, et al. Breast cancer survival and survival gap apportionment in sub-saharan Africa (ABC-DO): a prospective cohort study. Lancet Global Health. Sep 2020;8(9):e1203–12. https://doi.org/10.1016/S2214-109X(20)30261-8
5. Nounou MI, ElAmrawy F, Ahmed N, Abdelraouf K, Goda S, Syed-Sha-Qhattal H. Breast Cancer: Conventional Diagnosis and Treatment Modalities and Recent Patents and Technologies. Breast cancer: basic and clinical research. 2015;9(Suppl 2):17–34. https://doi.org/10.4137/BCBCR.S29420
6. Tomas CC, Oliveira E, Sousa D et al. May. Proceedings of the 3rd IPLeiria's International Health Congress: Leiria, Portugal. 6–7 2016. BMC health services research. Jul 6 2016;16 Suppl 3(Suppl 3):200. https://doi.org/10.1186/s12913-016-1423-5
7. Brand TC, Sawyer MM, King TA, Bolton JS, Fuhrman GM. Dec. Understanding patterns of failure in breast cancer treatment argues for a more thorough investigation of axillary lymph nodes in node negative patients. American journal of surgery. 2000;180(6):424-7. https://doi.org/10.1016/s0002-9610(00)00507-9
8. Gawde KA, Sau S, Tatiparti K et al. Paclitaxel and di-fluorinated curcumin loaded in albumin nanoparticles for targeted synergistic combination therapy of ovarian and cervical cancers. Colloids and surfaces B, Biointerfaces. Jul 1. 2018;167:8–19. https://doi.org/10.1016/j.colsurfb.2018.03.046
9. American College of Radiology. BI-RADS: ultrasound. 2nd ed. Reston, VA: American College of Radiology; 2013. Breast imaging reporting and data system atlas.
10. Boca Bene I, Ciurea AI, Ciortea CA, Dudea SM. Pros and Cons for Automated Breast Ultrasound (ABUS): A Narrative Review. Journal of personalized medicine. Jul 23. 2021;11(8). https://doi.org/10.3390/jpm11080703
11. Boca Bene I, Ciurea AI, Vesa SC, Ciortea CA, Dudea SM, Manole S. Associating Automated Breast Ultrasound (ABUS) and Digital Breast Tomosynthesis (DBT) with Full-Field Digital Mammography (FFDM) in Clinical Practice in Cases of Women with Dense Breast Tissue. Diagnostics. Feb 11. 2022;12(2). https://doi.org/10.3390/diagnostics12020459
12. Guldogan N, Yilmaz E, Arslan A, Kucukkaya F, Atila N, Aribal E. Aug. Comparison of 3D-Automated Breast Ultrasound With Handheld Breast Ultrasound Regarding Detection and BI-RADS Characterization of Lesions in Dense Breasts: A Study of 592 Cases. Academic radiology. 2022;29(8):1143–1148. https://doi.org/10.1016/j.acra.2021.11.022
13. Hatzipanagiotou ME, Huber D, Gerthofer V et al. Feb. Feasibility of ABUS as an Alternative to Handheld Ultrasound for Response Control in Neoadjuvant Breast Cancer Treatment. Clinical breast cancer. 2022;22(2):e142-e146. https://doi.org/10.1016/j.clbc.2021.05.010
14. Lin X, Jia M, Zhou X et al. Feb. The diagnostic performance of automated versus handheld breast ultrasound and mammography in symptomatic

outpatient women: a multicenter, cross-sectional study in China. European radiology. 2021;31(2):947–957. https://doi.org/10.1007/s00330-020-07197-7
15. Grady I, Chanisheva N, Vasquez T. Dec. The Addition of Automated Breast Ultrasound to Mammography in Breast Cancer Screening Decreases Stage at Diagnosis. Academic radiology. 2017;24(12):1570–1574. https://doi.org/10.1016/j.acra.2017.06.014
16. Gatta G, Cappabianca S, La Forgia D et al. Second-Generation 3D Automated Breast Ultrasonography (Prone ABUS) for Dense Breast Cancer Screening Integrated to Mammography: Effectiveness, Performance and Detection Rates. Journal of personalized medicine. Aug 31. 2021;11(9). https://doi.org/10.3390/jpm11090875
17. Kim SH, Kim HH, Moon WK. Jan. Automated Breast Ultrasound Screening for Dense Breasts. Korean journal of radiology. 2020;21(1):15–24. https://doi.org/10.3348/kjr.2019.0176
18. Hejduk P, Marcon M, Unkelbach J et al. Jul. Fully automatic classification of automated breast ultrasound (ABUS) imaging according to BI-RADS using a deep convolutional neural network. European radiology. 2022;32(7):4868–4878. https://doi.org/10.1007/s00330-022-08558-0
19. Cao X, Chen H, Li Y et al. Nov. Auto-DenseUNet: Searchable neural network architecture for mass segmentation in 3D automated breast ultrasound. Medical image analysis. 2022;82:102589. https://doi.org/10.1016/j.media.2022.102589
20. Cao X, Chen H, Li Y, Peng Y, Wang S, Cheng L. Jan. Uncertainty Aware Temporal-Ensembling Model for Semi-Supervised ABUS Mass Segmentation. IEEE transactions on medical imaging. 2021;40(1):431–443. https://doi.org/10.1109/TMI.2020.3029161
21. Cao X, Chen H, Li Y, Peng Y, Wang S, Cheng L. Sep. Dilated densely connected U-Net with uncertainty focus loss for 3D ABUS mass segmentation. Computer methods and programs in biomedicine. 2021;209:106313. https://doi.org/10.1016/j.cmpb.2021.106313
22. Lei Y, He X, Yao J et al. Jan. Breast tumor segmentation in 3D automatic breast ultrasound using Mask scoring R-CNN. Medical physics. 2021;48(1):204–214. https://doi.org/10.1002/mp.14569
23. Ma JJ, Meng S, Dang SJ et al. Evaluation of a new method of calculating breast tumor volume based on automated breast ultrasound. Frontiers in oncology. 2022;12:895575. https://doi.org/10.3389/fonc.2022.895575
24. Zhuang Z, Ding W, Zhuang S et al. Jun. Tumor classification in automated breast ultrasound (ABUS) based on a modified extracting feature network. Computerized medical imaging and graphics: the official journal of the Computerized Medical Imaging Society. 2021;90:101925. https://doi.org/10.1016/j.compmedimag.2021.101925
25. Zhou Y, Chen H, Li Y, Cao X, Wang S, Shen D. Jan. Cross-Model Attention-Guided Tumor Segmentation for 3D Automated Breast Ultrasound (ABUS) Images. IEEE journal of biomedical and health informatics. 2022;26(1):301–311. https://doi.org/10.1109/JBHI.2021.3081111
26. Zhang J, Tao X, Jiang Y et al. Application of Convolution Neural Network Algorithm Based on Multicenter ABUS Images in Breast Lesion Detection. Frontiers in oncology. 2022;12:938413. https://doi.org/10.3389/fonc.2022.938413
27. Cheng Z, Li Y, Chen H, Zhang Z, Pan P, Cheng L. Jun. DSGMFFN: Deepest semantically guided multi-scale feature fusion network for automated lesion segmentation in ABUS images. Computer methods and programs in biomedicine. 2022;221:106891. https://doi.org/10.1016/j.cmpb.2022.106891
28. Wang Q, Chen H, Luo G et al. Oct. Performance of novel deep learning network with the incorporation of the automatic segmentation network for diagnosis of breast cancer in automated breast ultrasound. European radiology. 2022;32(10):7163–7172. https://doi.org/10.1007/s00330-022-08836-x
29. Meng Z, Chen C, Zhu Y et al. Dec. Diagnostic performance of the automated breast volume scanner: a systematic review of inter-rater reliability/agreement and meta-analysis of diagnostic accuracy for differentiating benign and malignant breast lesions. European radiology. 2015;25(12):3638-47. https://doi.org/10.1007/s00330-015-3759-3
30. Girometti R, Zanotel M, Londero V, Linda A, Lorenzon M, Zuiani C. Mar. Automated breast volume scanner (ABVS) in assessing breast cancer size: A comparison with conventional ultrasound and magnetic resonance imaging. European radiology. 2018;28(3):1000–1008. https://doi.org/10.1007/s00330-017-5074-7
31. Schmachtenberg C, Fischer T, Hamm B, Bick U. Aug. Diagnostic Performance of Automated Breast Volume Scanning (ABVS) Compared to Handheld Ultrasonography With Breast MRI as the Gold Standard. Academic radiology. 2017;24(8):954–961. https://doi.org/10.1016/j.acra.2017.01.021
32. Giger ML, Inciardi MF, Edwards A et al. Jun. Automated Breast Ultrasound in Breast Cancer Screening of Women With Dense Breasts: Reader Study of Mammography-Negative and Mammography-Positive Cancers. AJR American journal of roentgenology. 2016;206(6):1341-50. https://doi.org/10.2214/AJR.15.15367
33. Liu J, Zhao H, Huang Y et al. Genome-wide cell-free DNA methylation analyses improve accuracy of non-invasive diagnostic imaging for early-stage breast cancer. Molecular cancer Feb 19. 2021;20(1):36. https://doi.org/10.1186/s12943-021-01330-w
34. van Zelst JCM, Tan T, Platel B et al. Apr. Improved cancer detection in automated breast ultrasound by radiologists using Computer Aided Detection. European journal of radiology. 2017;89:54–59. https://doi.org/10.1016/j.ejrad.2017.01.021
35. Xiang H, Huang YS, Lee CH et al. May. 3-D Res-CapsNet convolutional neural network on automated breast ultrasound tumor diagnosis. European journal of radiology. 2021;138:109608. https://doi.org/10.1016/j.ejrad.2021.109608
36. Zhao F, Cai C, Liu M, Xiao J. Identification of the lymph node metastasis-related automated breast volume scanning features for predicting axillary lymph node tumor burden of invasive breast cancer via a clinical prediction model. Frontiers in endocrinology. 2022;13:881761. https://doi.org/10.3389/fendo.2022.881761

Publisher's note